Journal of Atmospheric and Solar-Terrestrial Physics ▮ (▮▮▮▮) ▮▮▮–▮▮▮

Contents lists available at SciVerse ScienceDirect

Journal of Atmospheric and Solar-Terrestrial Physics

journal homepage: www.elsevier.com/locate/jastp

Inter-hemispheric coupling during northern polar summer periods of 2002–2010 using TIMED/SABER measurements

R.A. Goldberg [a,*], A.G. Feofilov [a,b], W.D. Pesnell [c], A.A. Kutepov [a,b]

[a] NASA Goddard Space Flight Center, Mailcode 674, Greenbelt Road, Greenbelt, MD 20771, USA
[b] The Catholic University of America, 620 Michigan Avenue, Washington D.C. 20064, USA
[c] NASA Goddard Space Flight Center, Mailcode 671, Greenbelt Road, Greenbelt, MD 20771, USA

ARTICLE INFO

Article history:
Received 7 May 2012
Received in revised form
18 November 2012
Accepted 26 November 2012

Keywords:
Inter-hemispheric-coupling
Polar summer
Stratospheric warming

ABSTRACT

It has been found that for more than one polar summer season between 2002 and 2010, the northern polar mesospheric region near and above about 80 km was warmer than normal. The strongest warming effect of this type was observed to occur during northern summer 2002. Observational and theoretical studies imply that these "anomalies" were preceded by unusual dynamical processes in the southern hemisphere. We have analyzed temperature distributions measured by the SABER limb scanning infrared radiometer aboard the NASA TIMED satellite between 2002 and 2010 at altitudes from 15 to 110 km and for latitudes between 83°S and 83°N. We describe the approach to trace the spatial extent of inter-hemispheric temperature correlations demonstrating the global features that were unique for the "anomalous" northern polar summers. From our analysis of SABER data from 2002 to 2010, the anomalous heating for the northern mesopause region during northern summer was accompanied by stratospheric heating in the equatorial region. In the winter hemisphere it is accompanied by heating in the lower stratosphere and mesopause region, and cooling in the stratopause region. Also, all the elements of the temperature anomaly structure appear to develop and fade away nearly simultaneously, thereby suggesting either a global influence or a short lagging period (less than 7 days).

1. Introduction

In July, 2002, the MaCWAVE/MIDAS rocket program (Goldberg et al., 2004) was conducted at Andøya Rocket Range, Norway (ARR, 69.3°N, 16°E) to study the influence of gravity waves (GWs) on the polar summer mesosphere. As part of that program, a large number of falling sphere MET payloads were launched to obtain the atmospheric temperature in the mesopause region. These data led to the conclusion that the mesopause temperatures were abnormally high above 80 km when compared to the mean value profiles for prior years. This was further evidenced by a reduced polar mesospheric summer echo (PMSE) occurrence rate as shown in Fig. 4 of Goldberg et al. (2004). This is to be expected since the echoes are thought to be related to charged ice particles with diameters in the nanometer range, with concentrations that decrease as the temperature heats up to the frost-point. Becker et al. (2004) proposed that this heating effect was a consequence of Rossby-wave forcing arising from the southern polar winter, particularly in the troposphere and stratosphere (here and below we use the term "heating" though a more correct term would be "reduced cooling" associated with weaker gravity wave forcing of the meridional circulation during warmer years). Later, Becker and Fritts (2006) expanded on this theoretical concept with a more refined model. More recently, Karlsson et al. (2009) have argued that the variability in the summer polar mesosphere is caused by the planetary wave flux entering the winter stratosphere. This was accomplished by using the Canadian Middle Atmosphere Model (CMAM). It involves cross-equatorial flow caused by a stratospheric warming in the southern hemisphere (SH).

In this work, we use temperature retrievals from the TIMED/SABER instrument to trace the inter-hemispheric coupling for the mesospheric heating event first observed locally during the MaCWAVE/MIDAS rocket program, which seemed to occur nearly simultaneously with a stratospheric warming in the southern winter polar stratosphere. We perform similar analyses for other years and compare the observed temperature anomalies with the current understanding of the mechanism of the inter-hemispheric coupling.

2. Background

The TIMED (Thermosphere, Ionosphere, Mesosphere Energetics and Dynamics) Satellite was launched by NASA on December 7, 2001, and has been operating continuously to the present time. The SABER (Sounding of the Atmosphere using Broadband

* Corresponding author.
E-mail address: richard.a.goldberg@nasa.gov (R.A. Goldberg).

1364-6826/$ - see front matter © 2012 Published by Elsevier Ltd. All rights reserved.
http://dx.doi.org/10.1016/j.jastp.2012.11.018

Emission Radiometry) instrument in TIMED provides profiles of kinetic temperature, pressure and density, as well as minor constituents such as CO_2, NO, O_3, H_2O. The latitudinal coverage is governed by a 60-day yaw cycle that allows observations of latitudes from 83°S to 52°N in the South viewing phase or from 53°S to 82°N in the North viewing phase. Temperatures obtained in each polar region are a major part of this study.

Measurements at ARR from meteorological rocket falling sphere payloads, showing the warm polar summer in the northern hemisphere (NH) above 80 km altitude during MaCWAVE/MIDAS, were reported by Goldberg et al. (2004, Fig. 3) and Rapp et al. (2004, Fig. 1d). Further evidence for this behavior was also observed from synoptic studies of polar mesospheric summer echoes (PMSEs) in Goldberg et al. (2004, Fig. 4). A more recent display of PMSEs measured at Andøya (Latteck, personal communication, 2008) is shown in Fig. 1. The PMSE figures both show that the frequency of occurrence of PMSEs and the duration of the season for occurrence were significantly lower during 2002 than for years following the 2002 season. Fig. 2 is a schematic to help explain why this is an important indicator for polar mesospheric warming. The figure defines the altitude region where PMSEs and polar mesospheric clouds (PMCs) would occur: given that there is a sufficient amount of gaseous water and ice nucleation centers, mesospheric ice particles start to form; as they grow large, they move to a lower and warmer part of the atmosphere and sublimate there, giving rise to water vapor under the cloud (Feofilov and Petelina, 2010). The occurrence and vertical extent of PMSEs rely on the temperature to be below the frost-point temperature. Clearly, a warming of this region would reduce the extent and possible occurrence of such phenomena. Further evidence regarding the warm polar summer of 2002 has been reported by Karlsson et al. (2009) and Feofilov and Petelina (2010), who showed a reduction in PMCs for the northern polar summer of 2002, using OSIRIS data from the Swedish ODIN satellite.

The mechanism of inter-hemispheric coupling has been a subject of numerous studies (Becker and Fritts, 2006; Karlsson et al., 2007, 2009; Xu et al., 2009; Körnich and Becker, 2010; Murphy et al., 2012). The latter work provides an overview of the current understanding of the mechanism, which is termed "BKK mechanism" after the names of the lead authors. The process is split into three stages: during the first stage, an increase in winter stratospheric wave activity leads to a decrease in strength of the zonal winds in the winter stratosphere. At the second stage, weaker zonal winds affect GW filtering and GW drag above the stratopause, resulting in weaker mesospheric circulation in the winter hemisphere, warming of the lower mesosphere in the tropical region, and its cooling in polar winter. Finally, during the third stage, the warming of the tropical lower mesosphere propagates

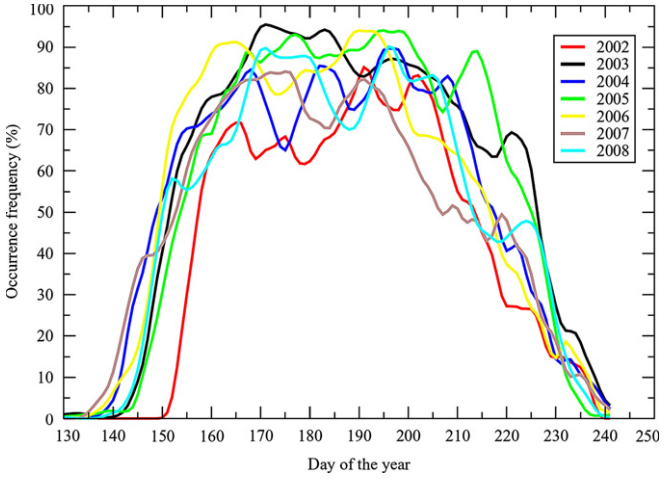

Fig. 1. Occurrence frequency of PMSE at ALOMAR from 2002 to 2008.

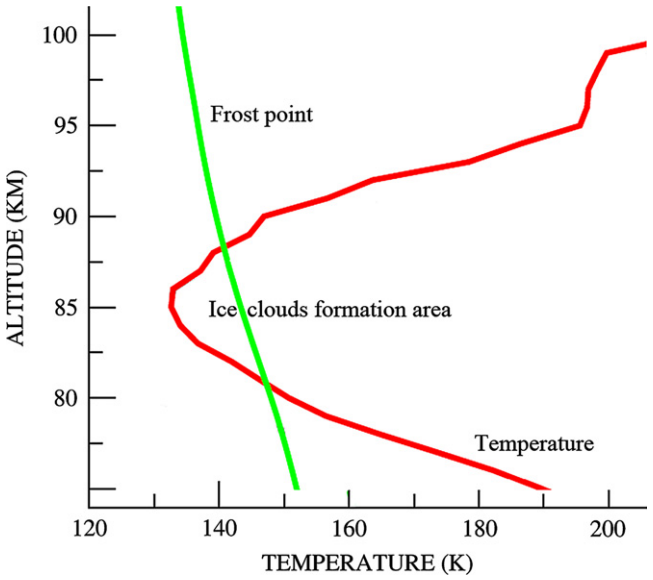

Fig. 2. Schematic illustrating how the frost point temperatures exceed the polar summer temperatures in the upper mesosphere thereby permitting formation of PMCs and PMSEs.

to the summer mesosphere. In addition, Espy et al. (2011) and Murphy et al. (2012) also considered the role of the quasi-biennial oscillation in modulating the inter-hemispheric coupling. In this work, we use 9 years of SABER temperature data, from 2002 to 2010, to trace inter-hemispheric coupling and, where possible, check the consistency of the observations with the aforementioned stages.

3. Instrumentation and approach

3.1. The SABER instrument onboard the TIMED satellite

The TIMED satellite was launched on December 7, 2001 into a 74.1° inclined 625 km orbit with a period of 1.7 h. The TIMED mission is focused on the energetics and dynamics of the mesosphere-lower thermosphere region (60–180 km) (Yee et al., 1999). SABER is a 10-channel broadband limb-scanning infrared radiometer covering the spectral range from 1.27 μm to 17 μm (Russell et al., 1999). SABER provides vertical profiles of kinetic temperature, pressure, ozone, carbon dioxide, water vapor, atomic oxygen, atomic hydrogen and volume emission rates in the NO (5.3 μm) and OH Meinel and $O_2(^1\Delta)$ bands. The vertical instantaneous field of view of the instrument is approximately 2.0 km at 60 km altitude, the vertical sampling interval is ~0.4 km, and the atmosphere is scanned from below the surface to 400 km tangent height. The instrument performs one complete up and down scan every 53 s. The instrument has been performing near-continuous measurements since January 25, 2002. The latitudinal coverage is governed by a 60-day yaw cycle that allows observations of latitudes from 83°S to 52°N in the South viewing phase or from 53°S to 82°N in the North viewing phase. It is important to note that the latitudinal coverage is consistent for all years: during the summer period in the NH, SABER changes from North viewing phase to South viewing phase on day 194.

3.2. Peculiarities of non-LTE temperature retrievals and retrieval errors

In this work we utilized version V1.07 of SABER data available online (http://saber.gats-inc.com/, last accessed on 16th November

2012). The detailed analysis of the quality of this dataset is given by Remsberg et al. (2008). Here we quote the root-mean-square error estimates for different altitudes provided there.

In Table 1, T_{polar} refers to polar summer temperature distributions and $\Delta T_{regular}$ represents error estimates at all other seasons and latitudes. As one can see, the errors in the polar summer mesopause region grow more rapidly above 85 km. This is linked with the mechanism of 15 μm CO_2 radiance forming and ratios between the components contributing to pumping the $CO_2(v_2)$. In the lower atmosphere the frequency of inelastic molecular collisions is sufficiently high, so that these collisions overwhelm other population/depopulation mechanisms of the molecular vibrational levels. This leads to a local thermodynamic equilibrium (LTE), and the populations follow the Boltzmann distribution governed by the local kinetic temperature T_{kin}. In the upper atmosphere, where the frequency of inelastic collisions is much less than at lower altitudes, other processes can influence the population of CO_2 vibrational levels. These include: (a) the direct absorption of solar radiance by the CO_2 vibrational-rotational bands in the 2.0, 2.7, and 4.3 μm spectral region; (b) absorption of the 15 μm radiance coming from the warmer and denser lower atmosphere; (c) vibrational–translational (V–T) energy exchanges by collisions with molecules and atoms of other atmospheric constituents; and (d) collisional vibrational–vibrational (V–V) energy exchange with other molecules. As a result, LTE no longer applies in this altitude region and the populations must be found by simultaneously solving the self-consistent system of kinetic equations that express the balance relations between various excitation/de-excitation processes and the radiative transfer equation. The polar summer temperature profile can be characterized by a steep gradient in the stratopause–mesopause region and extremely low (100–130 K) mesopause temperatures. Hence, the local thermal component of the $CO_2(v_2)$ level pumping is low in comparison with the radiance coming from below, the populations of these levels are in non-LTE starting at 72 km (Kutepov et al., 2006) and the temperature retrieval errors become larger. We will demonstrate, however, that the temperature anomalies

Table 1
Temperature uncertainties for SABER V1.07 dataset (from Remsberg et al., 2008).

Altitude (km)	15	20	30	40	50	60	70	80	85	90	95	100
$\Delta T_{regular}$ (K)	1.4	1.3	0.8	1.6	2.0	2.1	1.6	2.3	3.8	5.4	6.5	8.4
ΔT_{polar} (K)	1.4	1.3	0.8	1.6	2.0	2.1	1.6	5.3	8.2	10.4	16.4	25.8

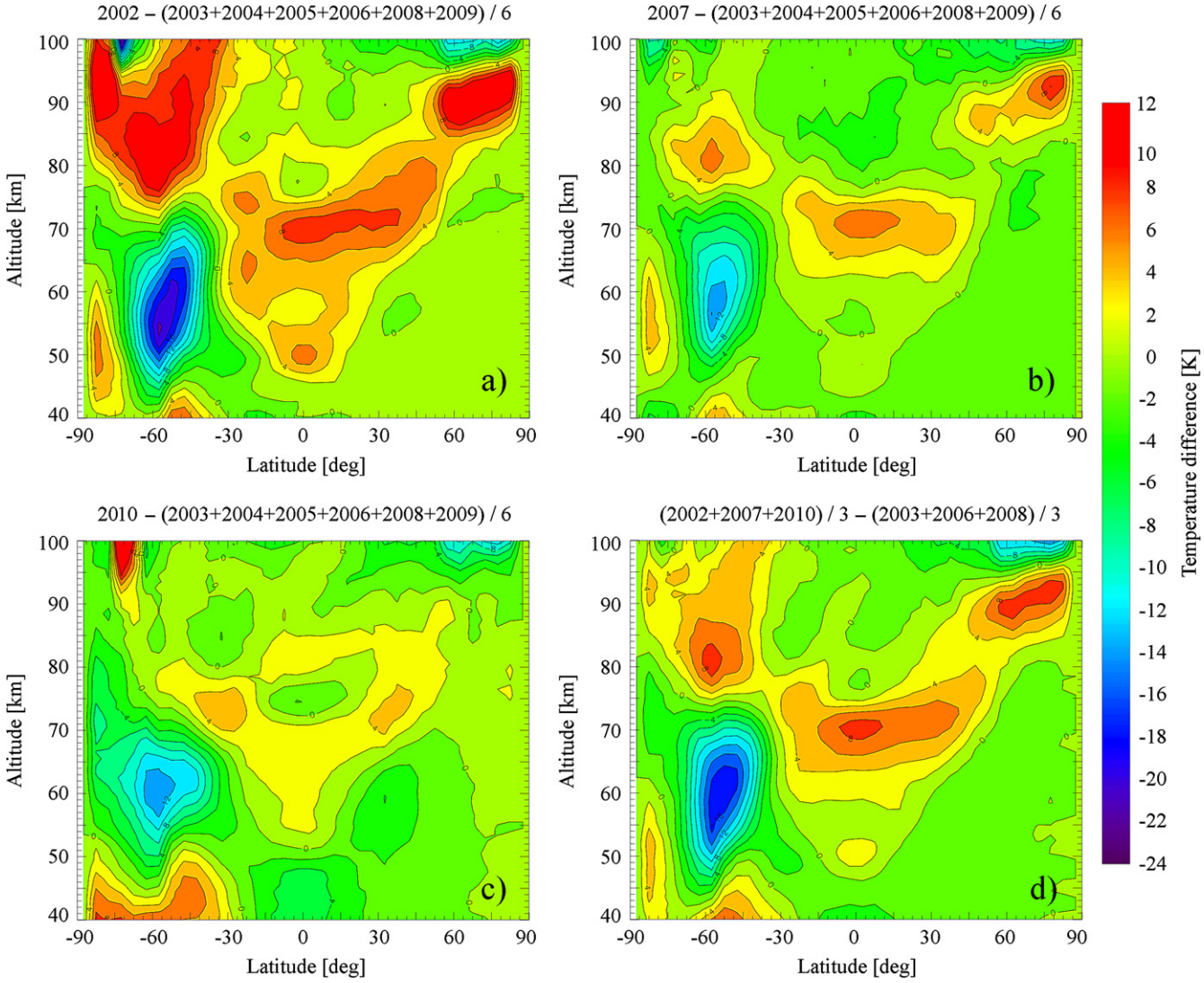

Fig. 3. Temperature anomalies in the period of 2002–2010 as seen by TIMED/SABER. Panels (a–c) are different maps of the strongest anomaly years minus the average of the six weakest years. Panel (d) is the three strongest-year average minus the three weakest-year average. For each year, days 182–212 were used to extend the latitudinal coverage.

Please cite this article as: Goldberg, R.A., et al., Inter-hemispheric coupling during northern polar summer periods of 2002–2010 using.... Journal of Atmospheric and Solar-Terrestrial Physics (2013), http://dx.doi.org/10.1016/j.jastp.2012.11.018

we observe exceed these errors. Moreover, since the uncertainties in the non-LTE rates that are responsible for the uncertainty of temperature retrievals from SABER measurements (Garcia-Comas et al., 2008) do not depend on the season or latitude, they do not introduce any bias in summer-to-summer correlative analysis performed in this work.

4. Results and discussion

As a first step we show the different maps of 31-day averaged SABER temperatures during the summers of 2002–2010 (Fig. 3). To extend the latitude coverage we have selected days 182–212, the period of time that included the yaw maneuver. This selection makes the averages consistent with those shown by Espy et al. (2011) that will be used below. The plots in Fig. 3 show temperature deviations from 83°S to 82°N. Latitudes 53°S–53°N were observed for the whole time interval considered, while the 53°N–82°N and 83°S–53°S areas were observed only during days 182–194 and 194–212, respectively. Both day- and night-time temperatures were zonally averaged and binned with a 5 degree latitude step and a 1 km altitude step. We identified "normal," "cold" and "warm" years with respect to the polar summer mesospheric area and built the differences in temperature distributions. Fig. 3a shows the temperature difference map for 2002, the warmest year, in comparison to the averaged (2003+2004+2005+2006+2008+2009)/6 temperature distribution. This panel demonstrates the pattern that can also be seen in other panels in Fig. 3: a warmer than usual summer polar mesopause area; a warmer tropical atmosphere in the approximate 65–75 km altitude range; and finally, warmer mesopause, colder stratopause and warmer lower stratospheric areas at high latitudes in the winter hemisphere. Temperature differences can reach 12 K in warm areas and 20 K in the cold areas. Besides 2002, the summers of 2007 and 2010 also demonstrated similar patterns (see Fig. 3b and c). Finally, Fig. 3d shows the temperature difference between the three warmest years versus the three coldest years.

It is interesting to compare the observed pattern with the theoretical schemes of the inter-hemispheric coupling in Körnich and Becker (2010). According to this scheme, strengthening of the circulation in the winter stratosphere and an anomaly of the planetary wave drag occurs in the winter stratosphere inducing a stronger Brewer–Dobson circulation and yielding an anomalously warm stratospheric winter pole and colder tropics. These features are partially seen in Fig. 3. The propagation of the equatorial mesospheric warming towards high latitudes and higher altitudes in the summer hemisphere, associated with a GW drag anomaly, is clearly seen. Overall, the temperature anomaly pattern in Fig. 3 is in good agreement with the pattern provided by the BKK mechanism of inter-hemispheric coupling.

To further study the development of the features seen in Fig. 3 for 2002 we have split the period of June and July into one-week intervals and traced the changes on this timescale. The nine panels in Fig. 4 demonstrate how the "anomalous" structure progressed from almost non-existent during the first week of June to its maximum in the June 28–July 4 period and then started fading after July 25. The dashed lines with arrows in Fig. 4 help track the behavior of temperature anomalies at different locations. It is important to note here that all the important elements of temperature anomaly structure seen in Fig. 3 and Fig. 4 appear to develop nearly *simultaneously* (we estimate the lag between SH and NH changes to be less than 7 days, the time step used in this study). We observed similar behavior for temperature anomalies in 2007 and 2010. We will now try to identify if these phenomena are linked, if changes in one region induce changes in the other, and if there is any periodicity in the observed anomalies.

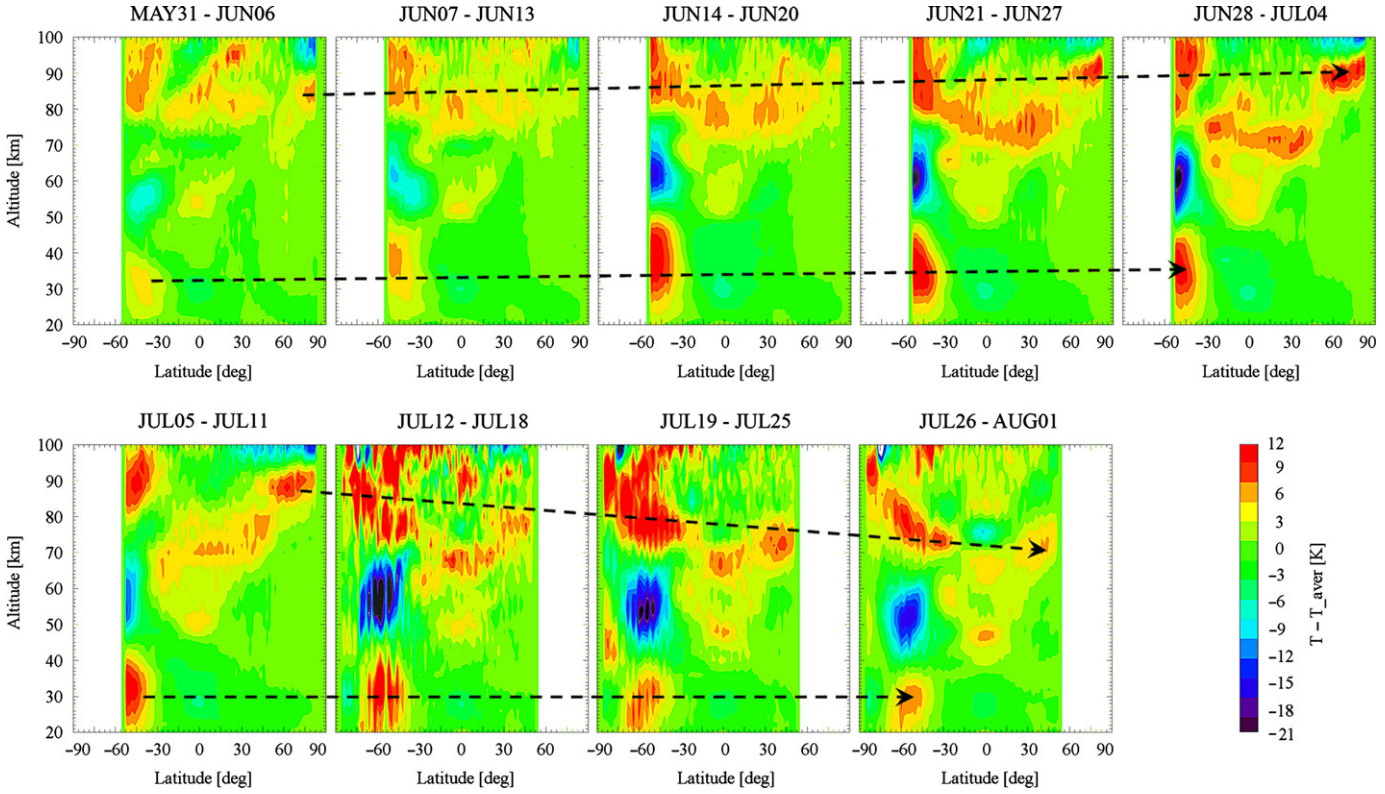

Fig. 4. Temperature anomaly development in June–July 2002. The $T-T_{ave}$ sequence is shown as weekly averages. The dashed lines track the persistence in space and time of each warm event.

Please cite this article as: Goldberg, R.A., et al., Inter-hemispheric coupling during northern polar summer periods of 2002–2010 using.... Journal of Atmospheric and Solar-Terrestrial Physics (2013), http://dx.doi.org/10.1016/j.jastp.2012.11.018

Next, we consider geopotential height differences as a visualization for polar vortex breakup. To test the hypothesis of sudden stratospheric warming (SSW) in the winter hemisphere affecting the upper mesosphere/lower thermosphere in both hemispheres (Becker et al., 2004; Becker and Fritts, 2006; Karlsson et al., 2009; Mbatha et al., 2010) initiating the warming of both hemispheres we chose the 10 hPa geopotential height difference between maximum and minimum at one altitude, $\Delta h_{\mathrm{geopot}}$ (10 hPa), as a tracker of an SSW. This approach is explained by a typical behavior of geopotential height distribution during and after polar vortex breakdown followed by SSW: both in the case of vortex displacement and vortex splitting SSWs the 10 hPa isosurface shows distinctive maxima and minima located approximately at the same latitude. The stronger the breakdown, the larger the difference of geopotential heights. Fig. 5 demonstrates the behavior of $\Delta h_{\mathrm{geopot}}$ (10 hPa) for all 9 years and for all latitudes. The alternating coverage of the geopotential height is caused by the yaw of the TIMED satellite every 60 days, as discussed earlier. The $\Delta h_{\mathrm{geopot}}$ (10 hPa) values shown in Fig. 5 were calculated for each day in latitudinal belts of 10° width. One can see that 2002 was, indeed, a unique year with respect to $\Delta h_{\mathrm{geopot}}$ (10 hPa): the difference between maximal and minimal values of h_{geopot} (10 hPa) reached 4 km at 70°S on day 240. The other years demonstrated lower values of $\Delta h_{\mathrm{geopot}}$ (10 hPa) and one can see that there is no correlation between this parameter and "warm"/"cold" years (see discussion of Fig. 4 above). Moreover, even in 2002 the main effects of polar vortex breakup in the SH began after day 200 while the strongest warming in the polar summer mesosphere occurred during days 175–185 (Fig. 4), *well before* the critical warming event in the SH. Consequently, the SSW in the winter hemisphere cannot be considered as the cause of the warming in the polar summer mesosphere under study in 2002. Fig. 5 shows that similar vortex disturbances in the SH occurred in 2005, 2007, and possibly 2009, but always too late to affect the summer polar mesosphere in the NH. This result is in agreement with the recent work of Tan et al. (2012), where the teleconnection patterns for the cases with and without SSW are the same in the NH.

Another approach to temperature anomaly analysis is made by comparing the average summer temperatures at "turning points;" i.e., at the tropopause, which is at the lower boundary of SABER measurements, and at the stratopause and mesopause. The latitudes for this analysis should represent high latitudes in both hemispheres as well as tropical latitudes to trace the cross-equator correlations if they do exist. For this activity, the whole SABER V1.07 dataset was processed and zonal average temperature values for days 182–212 were calculated for the mesopause (T_{mesop}), stratopause (T_{stratop}), and tropopause or the lowest point in the SABER altitude scan (T_{tropop}). These were obtained for the 40°S–55°S, 5°S–5°N, and 65°N–75°N latitude belts. A linear fit to the corresponding temperature values

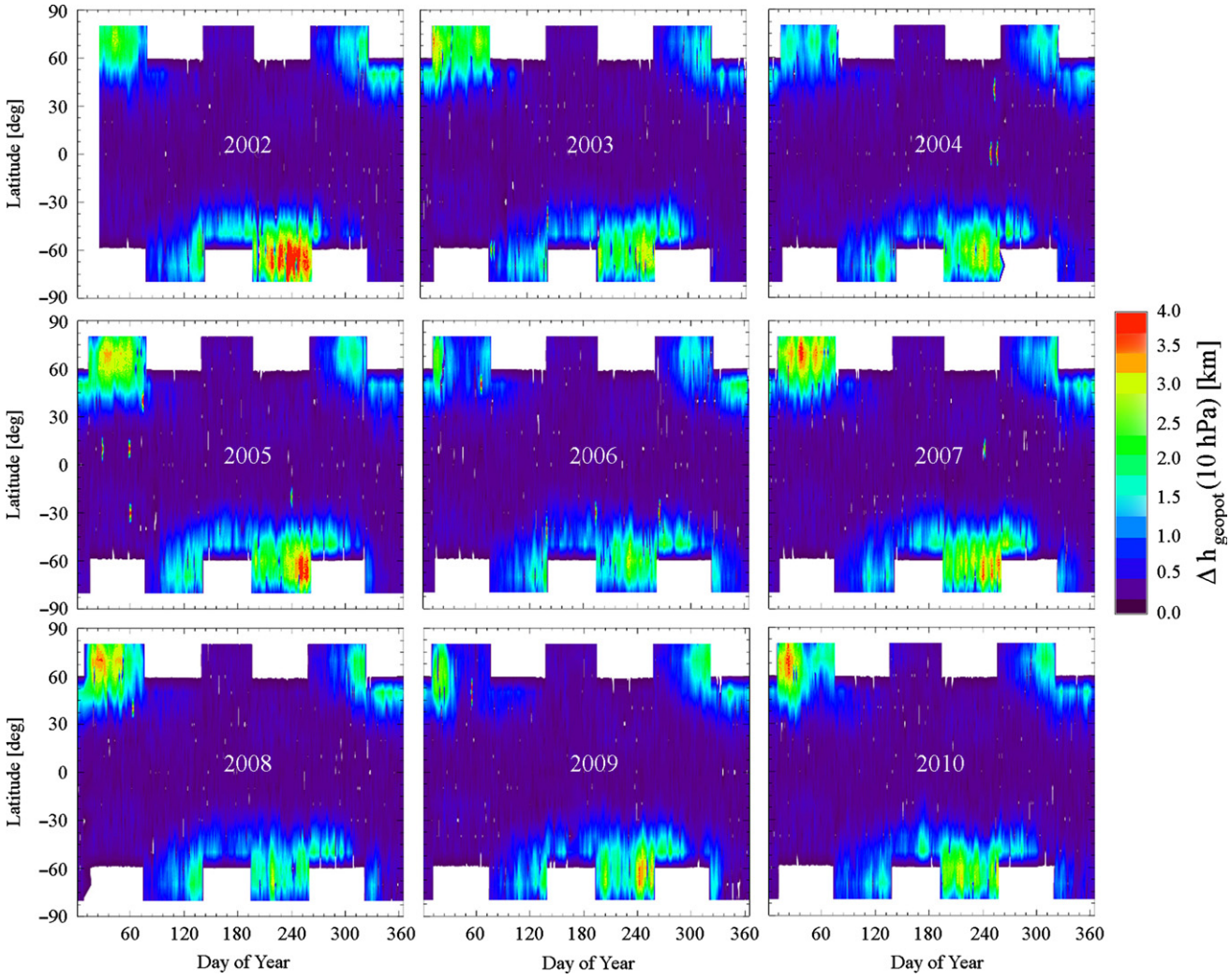

Fig. 5. Annual plots of the geopotential height differences ($\Delta h_{\mathrm{geopot}}$) designating a polar breakup causing a SSW. For each latitude, $\Delta h_{\mathrm{geopot}}$ is calculated as a difference in 10 hPa level height at this latitude.

Please cite this article as: Goldberg, R.A., et al., Inter-hemispheric coupling during northern polar summer periods of 2002–2010 using.... Journal of Atmospheric and Solar-Terrestrial Physics (2013), http://dx.doi.org/10.1016/j.jastp.2012.11.018

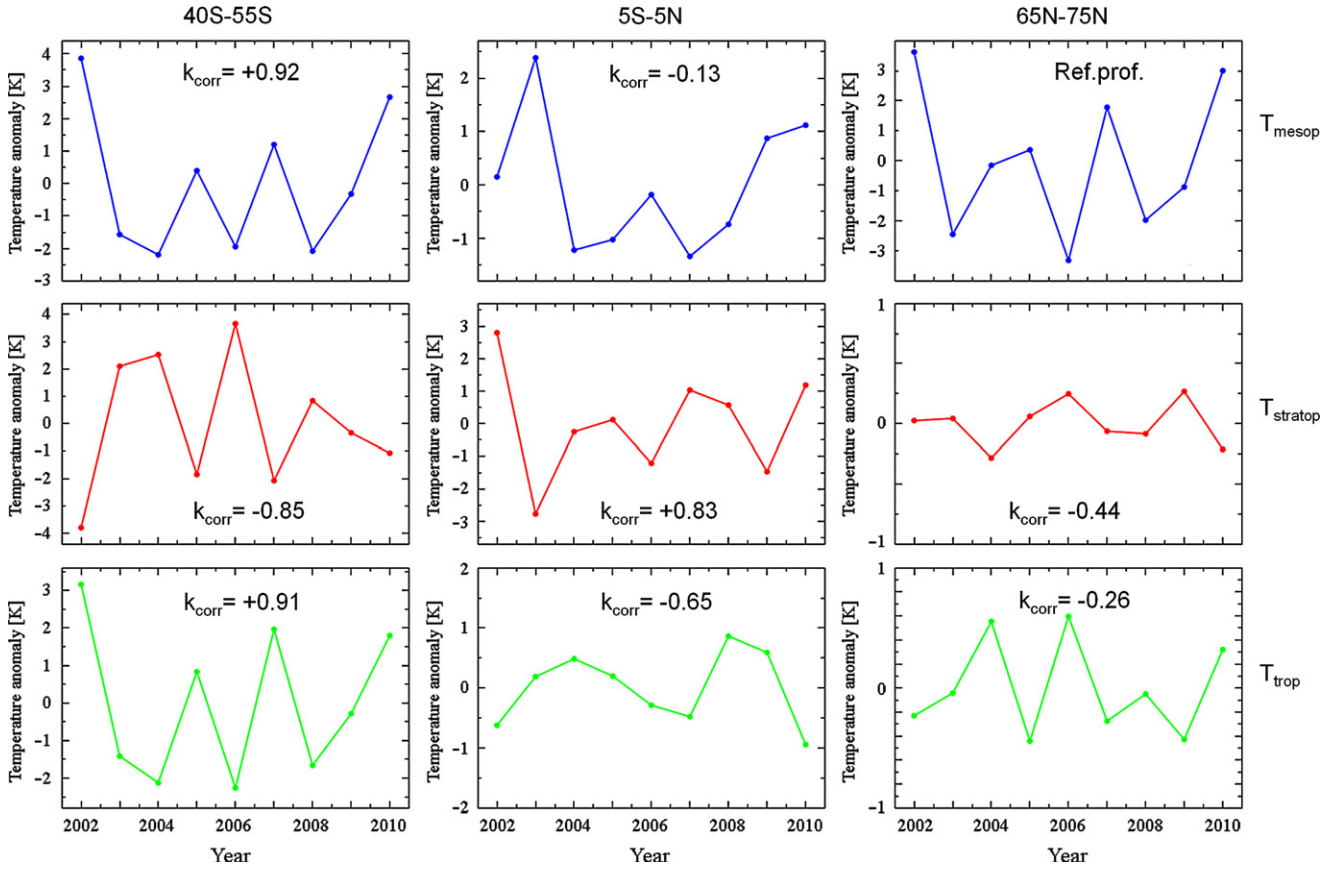

Fig. 6. Correlations of T_{mesop}, $T_{stratop}$, and T_{trop} for DOY 182–212 for each year from 2002 to 2010. The correlations are referenced to the T_{mesop} in the northern hemisphere. The southern hemisphere correlations are for lower latitudes due to the geographic sampling of the SABER instrument.

was made and subtracted to remove the long term trends. The remaining temperature anomalies for all 9 years analyzed are shown in Fig. 6. One can see that the temperature anomaly amplitudes are different for the atmospheric areas shown in Fig. 6; i.e., they vary from ± 0.3 K for $T_{stratop}$ in the summer hemisphere to ± 4.0 K for $T_{stratop}$ in the winter hemisphere. To analyze the year-to-year variability we have selected the polar summer T_{mesop} to be the "Reference." Fig. 6 illustrates how the average temperatures for days 182–212 correlate with other parts of the atmosphere. We have built linear correlation coefficients, k_{corr}, for each of the temperature anomalies shown in Fig. 6 with the reference T_{mesop} anomaly and put the k_{corr} values in the corresponding panels of Fig. 6. As one can see, the largest correlation coefficients are for the combination of polar summer T_{mesop} with tropical T_{mesop} (+0.83; significance 0.006) and mid-latitude T_{tropop} (+0.91; 0.0007), $T_{stratop}$ (−0.85; 0.004), and T_{mesop} (+0.92; 0.0005). These observations are consistent with the temperature differences seen in Fig. 3 and discussed earlier in this section. They are also consistent with the work of Karlsson et al. (2009), but expand that work to more regions of the atmosphere.

Since the correlation coefficients for the sequences in Fig. 6 are quite large, we will refer now only to the polar summer T_{mesop} that is shown in Fig. 7. This figure provides an expanded view of the polar summer T_{mesop} anomaly (line with circles) supplemented with the 30 hPa zonal wind anomaly curve (http://www.cpc.ncep.noaa.gov, last accessed on 11th March 2012) to test the recent hypothesis of Espy et al. (2011) regarding the QBO modulation of inter-hemispheric summer mesospheric temperatures coupling in years 1991–2000. Indeed, the temperature anomaly seen in Fig. 7 demonstrates periodic behavior. However, one can see that the period of the polar summer T_{mesop} anomaly curve in 2002–2010 does not match that of the QBO curve (~26–28 months, Baldwin et al., 2001; Fischer and Tung, 2008). Analysis of the QBO period from 2002 to 2010 shows a period of 26.4 months, nearer the lower limit of the 26–28 month period. It is obvious that the temperature anomaly values in Fig. 7 fit some periodic function. We have performed the search for this function, using period and phase as variable parameters. In Fig. 8 we show the behavior of the correlation coefficient (k_{corr}) and χ^2 deviation

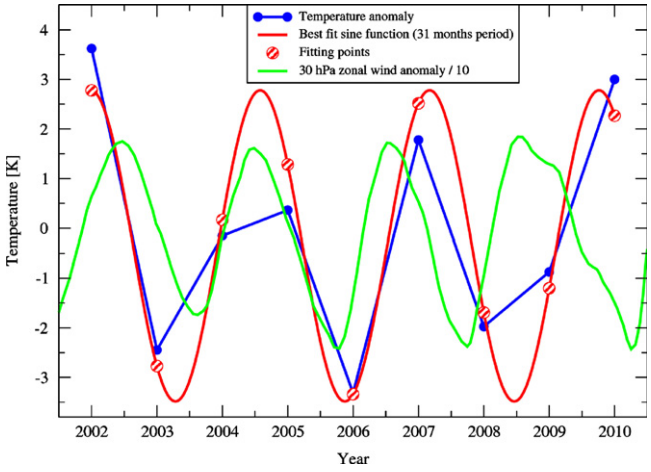

Fig. 7. Fitting the polar summer mesospheric temperature anomaly. Blue circles represent temperature anomaly values. Red curve shows the best fitting harmonic function (correlation coefficient k_{corr}=0.97) with a period of 31 months. The fitting has been performed at the points marked by red circles with stripes. Green curve corresponds to zonal wind anomaly as reported by the U. S. National Climate Center.

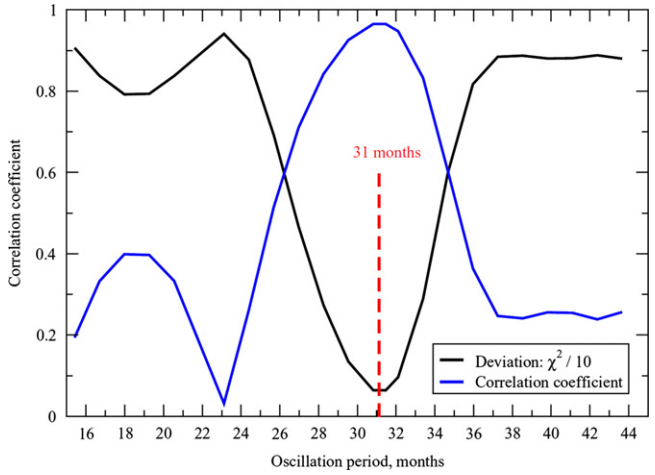

Fig. 8. On search of the oscillation period for the temperature anomaly at the northern mesopause. The correlation coefficient k_{corr} between the sequences shown by blue circles and red circles with stripes in Fig. 7 is built as a function of period of harmonic fitting function. Similarly, the χ^2 deviation between observed and simulated temperature anomalies is shown for different periods. Both curves demonstrate the best fitting of the observed temperature anomaly for oscillation period of ~31 months.

for two sets of values: reference temperature anomaly points retrieved from SABER measurements (blue dots in Fig. 7) and temperature anomalies approximated by a periodic function. As one can see, the maximum value of $k_{corr}=0.97$ is reached if the period is equal to 31 months. At the same time, this period also minimizes the χ^2 deviation. Fig. 7 shows that the QBO wind anomalies (green curve) and the periodic function, which fits the SABER temperature anomalies (red curve), are in phase for the period of 2004–2006 and in counter phase for the period of 2008–2010. This would tend to negate the QBO as a modulator of the effect, at least between 2002 and 2010.

5. Concluding remarks

The SABER pressure/temperature dataset for 2002–2010 was analyzed based on the MaCWAVE/MIDAS discovery of a warm summer polar mesosphere above approximately 83 km during 2002. Similar temperature anomalies in the northern polar mesosphere were also observed for the summers of 2007 and 2010. Overall, the observed temperature anomaly pattern follows the currently accepted model of inter-hemispheric coupling by Körnich and Becker (2010). We did not observe correlations between vortex disturbances in the SH and the temperature anomaly structures. For 2002, there was a large sudden stratospheric warming in the SH, but it followed rather than preceded the mesospheric warming in the NH. The elements of the observed temperature anomaly develop nearly simultaneously and the time lag, if any, can be estimated to be less than 7 days, the shortest time step used in our analysis.

We studied the 9-year period statistically (Fig. 6) and found that the behavior of the southern polar winter tropopause and mesopause correlated well with the equatorial stratopause and the northern polar summer on an annual basis. In the work of Espy et al. (2011) it was suggested that the inter-hemispheric coupling was modulated by the QBO, which had a period for their decade of study (1990–2000) of about 24.5 months. Our study for 2002–2010 occurred during a period when the QBO exhibited a period of about 26–28 months. However, the period of the temperature anomaly was very close to 31 months (Fig. 8), which does not appear to be directly influenced by the QBO. The explanation requires either a varying time lag or a beating against another oscillation not yet defined.

Acknowledgments

The work of A. Feofilov and A. Kutepov was supported by NASA grant NNX08AL12G. The authors thank two anonymous reviewers for their thoughtful comments on the manuscript and Alexander Medvedev for the discussion on atmospheric circulation mechanisms.

References

Baldwin, M.P., Gray, L.J., Dunkerton, T.J., Hamilton, K., Haynes, P.H., Randel, W.J., Holton, J.R., Alexander, M.J., Hirota, I., Horinouchi, T., Jones, D.B.A., Kinnersley, J.S., Marquardt, C., Sato, K., Takahashi, M., 2001. The quasi-biennial oscillation. Reviews of Geophysics 39, 179–229.

Becker, E., Müllemann, A., Lübken, F.-J., Körnich, H., Hoffmann, P., Rapp, M., 2004. High Rossby-wave activity in austral winter 2002: modulation of the general circulation of the MLT during the MaCWAVE/MIDAS northern summer program. Geophysical Research Letters 31, L24S08, http://dx.doi.org/10.1029/2004GL019615.

Becker, E., Fritts, D.C., 2006. Enhanced gravity-wave activity and interhemispheric coupling during the MaCWAVE/MIDAS northern summer program 2002. Annales Geophysicae 24, 1175–1188.

Espy, P.J., Fernández, S.O., Forkman, P., Murtagh, D., Stegman, J., 2011. The role of the QBO in the inter-hemispheric coupling of summer mesospheric temperatures. Atmospheric Chemistry and Physics 11, 495–502, http://dx.doi.org/10.5194/acp-11-495-2011.

Feofilov, A.G., Petelina, S.V., 2010. Relation between mesospheric ice clouds, temperature, and water vapor determined from Odin/OSIRIS and TIMED/SABER data. Journal of Geophysical Research 115, D18305, http://dx.doi.org/10.1029/2009JD013619.

Fischer, P., Tung, K.K., 2008. A reexamination of the QBO period modulation by the solar cycle. Journal of Geophysical Research 113, D07114, http://dx.doi.org/10.1029/2007JD008983.

Garcia-Comas, M., Lopez-Puertas, M., Marshall, B.T., Wintersteiner, P.P., Funke, B., Bermejo-Pantaleon, D., Mertens, C.J., Remsberg, E.E., Gordley, L.L., Mlynczak, M.G., Russell III, J.M., 2008. Errors in Sounding of the Atmosphere using Broadband Emission Radiometry (SABER) kinetic temperature caused by non-local-thermodynamic-equilibrium model parameters. Journal of Geophysical Research 113, D24106, http://dx.doi.org/10.1029/2008JD010105.

Goldberg, R.A., Fritts, D.C., Williams, B.P., Lübken, F.-J., Rapp, M., Singer, W., Latteck, R., Hoffman, P., Müllemann, A., Baumgarten, G., Schmidlin, F.J., She, C.-Y., Krueger, D.A., 2004. The MaCWAVE/MIDAS rocket and ground-based measurements of polar summer dynamics: overview and mean state structure. Geophysical Research Letters 31, L24S02, http://dx.doi.org/10.1029/2004GL019411.

Karlsson, B., Körnich, H., Gumbel, J., 2007. Evidence for interhemispheric stratosphere-mesosphere coupling derived from noctilucent cloud properties. Geophysical Research Letters 34, L16806, http://dx.doi.org/10.1029/2007GL030282.

Karlsson, B., McLandress, C., Shepherd, T.G., 2009. Inter-hemispheric mesospheric coupling in a comprehensive middle atmosphere model. Journal of Atmospheric and Terrestrial Physics 71, 518–530, http://dx.doi.org/10.1016/j.jastp.2008.08.006.

Körnich, H., Becker, E., 2010. A simple model for the interhemispheric coupling of the middle atmosphere circulation. Advanced Space Research 45, 661–668.

Kutepov, A.A., Feofilov, A.G., Marshall, B.T., Gordley, L.L., Pesnell, W.D., Goldberg, R.A., Russell III, J.M., 2006. SABER temperature observations in the summer polar mesosphere and lower thermosphere: importance of accounting for the CO_2 v_2 quanta V–V exchange. Geophysical Research Letters 33, L21809, http://dx.doi.org/10.1029/2006GL026591.

Mbatha, N., Sivakumar, V., Malinga, S.B., Bencherif, H., Pillay, S.R., 2010. Study on the impact of sudden stratosphere warming in the upper mesosphere-lower thermosphere regions using satellite and HF radar measurements. Atmospheric Chemistry and Physics 10, 3397–3404.

Murphy, D.J., Alexander, S.,.P., Vincent, R.A., 2012. Interhemispheric dynamical coupling to the southern mesosphere and lower thermosphere. Journal of Geophysical Research 117, D08114, http://dx.doi.org/10.1029/2011JD016865.

Rapp, M., Strelnikov, B., Müllemann, A., Lübken, F.-J., Fritts, D.C., 2004. Turbulence measurements and implications for gravity wave dissipation during the MaCWAVE/MIDAS rocket program. Geophysical Research Letters 31, L24S07, http://dx.doi.org/10.1029/2003GL019325.

Remsberg, E.E., Marshall, B.T., Garcia-Comas, M., Krueger, D., Lingenfelser, G.S., Martin-Torres, J., Mlynczak, M.G., Russell III, J.M., Smith, A.K., Zhao, Y., Brown, C., Gordley, L.L., Lopez-Gonzalez, M.J., Lopez-Puertas, M., She, C.-Y., Taylor, M.J., Thompson, R.E., 2008. Assessment of the quality of the Version 1.07 temperature-versus-pressure profiles of the middle atmosphere from TIMED/SABER. Journal of Geophysical Research 113, D17101, http://dx.doi.org/10.1029/2008JD010013.

Russell III, J.M., Mlynczak, M.G., Gordley, L.L., Tansock, J.J., Esplin, R., 1999. Overview of the SABER experiment and preliminary calibration results.

Proceedings of SPIE, Optical Spectroscopic Techniques and Instrumentation for Atmospheric and Space Research III 3756, 277–288.

Tan, B., Chu, X., Liu, H.-L., Yamashita, C., Russell III, J.M., 2012. Zonal-mean global teleconnection from 15 to 110 km derived from SABER and WACCM. Journal of Geophysical Research 117, D10106, http://dx.doi.org/10.1029/2011JD016750.

Xu, X., Manson, A.H., Meek, C.E., Chshyolkova, T., Drummond, J.R., Hall, C.M., Riggin, D.M., Hibbins, R.E., 2009. Vertical and interhemispheric links in the stratosphere-mesosphere as revealed by the day-to-day variability of Aura-MLS temperature data. Annales Geophysicae 27, 3387–3409.

Yee, J.-H., Cameron, G.E., Kusnierkiewicz, D.Y., 1999. Overview of TIMED. Proceedings of SPIE, Optical Spectroscopic Techniques and Instrumentation for Atmospheric and Space Research III 3756, 244–254.

Please cite this article as: Goldberg, R.A., et al., Inter-hemispheric coupling during northern polar summer periods of 2002–2010 using.... Journal of Atmospheric and Solar-Terrestrial Physics (2013), http://dx.doi.org/10.1016/j.jastp.2012.11.018